NANO LETTERS

pubs.acs.org/NanoLett Letter

# Rationally Designed Polymer Conjugate for Tumor-Specific Amplification of Oxidative Stress and Boosting Antitumor Immunity

Sheng Ma, Wantong Song,* Yudi Xu, Xinghui Si, Shixian Lv, Yu Zhang, Zhaohui Tang, and Xuesi Chen*

Cite This: https://dx.doi.org/10.1021/acs.nanolett.9b05265 Read Online

ACCESS | Metrics & More | Article Recommendations | Supporting Information

**ABSTRACT:** The crosstalk between tumor and stroma cells is a central scenario in the tumor microenvironment (TME). While the predominant effect of tumor cells on immune cells is establishing an immunosuppressive context, tumor cell death at certain conditions will boost antitumor immunity. Herein, we report a rationally designed tumor specific enhanced oxidative stress polymer conjugate (TSEOP) for boosting antitumor immunity. The TSEOP is prepared by Passerini reaction between cinnamaldehyde (CA), 4-formylbenzeneboronic acid pinacol ester, and 5-isocyanopent-1-yne, followed by azide–alkyne click reaction with poly(L-glutamic acid)-*graft*-poly(ethylene glycol) monomethyl ether (PLG-*g*-mPEG). Under tumor stimuli condition, CA and quinone methide (QM) are quickly generated, which cooperatively induce strong oxidative stress, immunogenic tumor cell death (ICD), and activation of antigen presenting cells. *In vivo* studies show that the TSEOP treatment boosts tumor-specific antitumor immunity and eradicates both murine colorectal and breast tumors. This study should be inspirational for designing polymers as immunotherapeutics in cancer therapy.

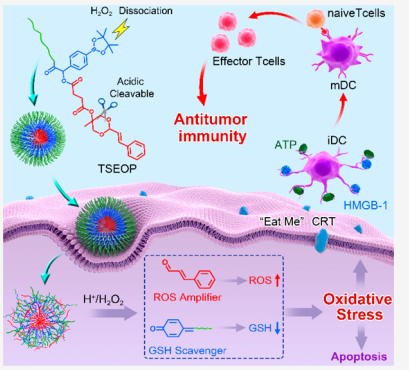


**KEYWORDS:** *Polypeptide, oxidative stress, immunogenic cell death, immunotherapy*



Crosstalk between tumor and the immune cells plays an important role in tumor progression and immune surveillance.[1,2] Immune cells like tumor-associated macrophages (TAMs) secrete various growth factors and cytokines for promoting tumor cell proliferation,[3] enhancing cell spreading,[4] stimulating blood vessel growth and angiogenesis,[5] and triggering TME changes.[6] At the same time, tumor cells also secrete cytokines for adjusting the immunophenotype of the immune cells into immunosuppressive type,[7] and enhance the expression of immunonegative regulating molecules for preventing the killing by immune cells.[8,9] Interestingly, recent studies found that some therapy-induced cell death would elicit tumor cell specific antitumor immunity, which may constitute one important reason for many successful anticancer interventions.[10] This kind of immunogenic cell death (ICD) is usually a result of therapy-induced extensive cellular stress and is characterized by active or passive release of cell death-associated molecular patterns (DAMPs).[11,12] These DAMPs can be sensed by corresponding pattern recognition receptors (PRRs) on tumor-infiltrating antigen presenting cells,[13] and they activate the immune system for tumor specific immune clearance.[14] If the ICD effect could be selectively amplified inside a tumor, the tumor growth may be inhibited by recovery of the immunosurveillance, and long-term inhibition may be realized for activation of the tumor-specific antitumor immunity.[15]

Several biochemical markers have been identified for correlating with ICD, including the exposure of calreticulin (CRT) on the surface of dying cells,[16] the release of large amounts of adenosine triphosphate (ATP),[17] and high-mobility group box 1 (HMGB1) into the extracellular milieu.[18] CRT represents the most abundant protein of the ER lumen.[19] Translocation of CRT from the ER lumen to the surface of cells is often associated with ER stress responses, which involves the phosphorylation of the eukaryotic translation initiation factor eIF2$\alpha$, followed by anterograde transport of CRT from the ER to the Golgi apparatus, the exocytosis of CRT-containing vesicles, and eventually the translocation of CRT onto the plasma membrane surface.[20] In most occasions, ER stress is featured with increased concentration of intracellular ROS and increased cytosolic $Ca^{2+}$ concentrations.[21] Therefore, selectively increasing intracellular ROS levels in tumor cells for enhancing the oxidative stress may be a meaningful way for inducing ICD and stimulating antitumor immunity.[22,23]

So far, several small molecule chemo drugs (e.g., doxorubicin, oxaliplatin),[24,25] photodynamic therapy (PDT),[26] and ionizing radiation[27] have been reported for inducing ICD by increasing intracellular ROS,[28,29] and the combination of them with other immunotherapeutics has

Received: December 23, 2019
Revised: February 14, 2020
Published: February 28, 2020

shown great potency in cancer therapy.[30,31] However, chemo drugs are cytotoxic to tumor cells as well as the immune cells, and the depth of penetration of visible light needed for activation of photosensitizers restricts the application PDT to only superficial skin cancers.[32] There are a number of recent reports concerning the modulation of tumor oxidative stress with polymer prodrugs or nanodelivery systems for cancer treatment,[33−37] and these studies may provide new potential options for inducing ICD and antitumor immunity. On the basis of these considerations, we designed a TSEOP for cooperative amplifiation of oxidative stress in tumor cells, and expect to use such polymer as a tumor-specific immunotherapeutic for boosting antitumor immunity (Scheme 1).

**Scheme 1. TSEOP for Inducing ICD and Boosting Antitumor Immunity**[a]

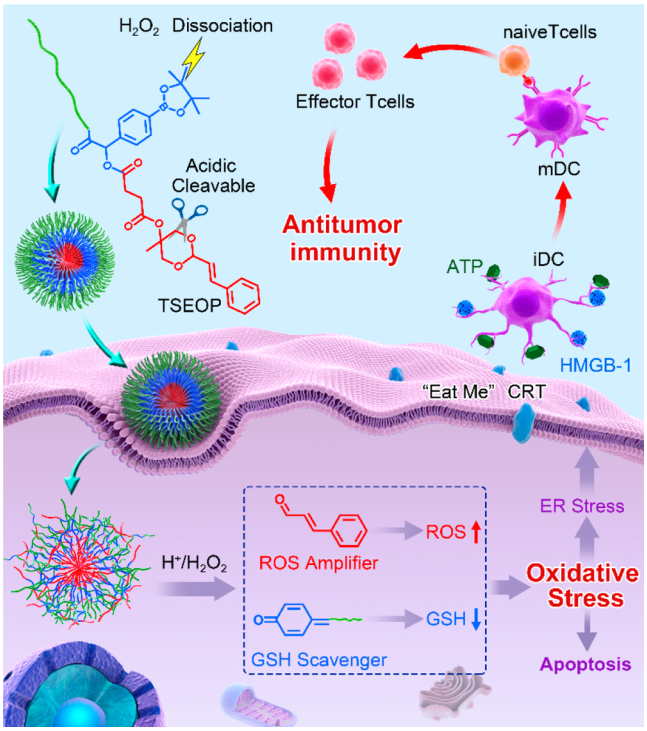


[a]Upon uptake by tumor cells, TSEOP will generate CA and QM, serving as a ROS amplifier and a GSH scavenger, respectively. This cooperative interaction between CA and QM induces strong oxidative and ER stress, ICD, and subsequent activation of immature dendritic cells (iDCs). Matured DCs (mDCs) present tumor-associated antigens to naïve T cells to stimulate the generation of effector T cells, resulting in enhanced antitumor immunity.

**Results and Discussion.** The TSEOP was prepared by conjugation of phenylboronic acid containing CA derivatives (PBCA) onto PLG-*g*-mPEG (Figure 1A). PBCA (4) was synthesized by Passerini reaction between carboxyl-terminated acetal bond modified CA (1) with 4-formylphenylborate pinacol ester (2) and 5-isocyanopent-1-yne (3) in $CHCl_3$. The carboxyl-terminated acetal bond modified CA was obtained by two steps: CA was first reacted with tris(hydroxymethyl)-ethane through aldol condensation reaction to form an acetal bond, and the newly formed methine protons (*d*) of acetal bond at $\delta$ 5.05−5.07 (d, 1H) ppm proved the existence of acetal linkage (Figure S1); then acetal bond modified CA was further reacted with succinic anhydride to get carboxyl-terminated CA derivatives, the newly formed carboxyl protons (*i*) at $\delta$ 12.2 (s, 1H) ppm, and methylene protons (*h*) at $\delta$ 2.55−2.59 (m, 4H) ppm proved the existence of carboxyl group (Figure S2). Carboxyl-terminated acetal bond modified CA further reacted with 4-formylphenylborate pinacol ester and 5-isocyanopent-1-yne (Passerini three component reaction) and resulted in PBCA. Successful synthesis of PBCA was confirmed by the appearance of the methine protons (*j*) of the *p*-boronabenzyl ester at $\delta$ 6.08 (s, 1H) ppm in $CDCl_3$ (Figure S5). The PLG-*g*-mPEG was developed previously by our group and had been shown to have long blood circulation time and good stability *in vivo*.[38] For effective conjugation with PBCA, PLG-*g*-mPEG was first modified with azapropylamine to obtain PLG-*g*-mPEG/azidopropylamine (PLG-$N_3$) (5) (Figure S6) and then PBCA was conjugated with PLG-*g*-mPEG via click reaction to obtain the final TSEOP (6) (Figures 1A and S7). The number-average molecular weight ($M_n$) of TSEOP is 81.6k Da with polydispersion index of 1.69 (Figure S8). Because of the amphiphilic property of the structure, TSEOP formed nanostructures in pH 7.4 solution, with a hydrodynamic radius ($R_h$) of about 40 nm (Figure S9A). The self-assembled TSEOP nanomicelles presented the uniform size and spherical morphologies in pH 7.4 solution (Figure S9B).

The $H_2O_2$-triggered release of QM and acid-triggered generation of CA from PBCA was monitored by $^1$H NMR analysis. The degradation was investigated in a mixture of DMSO-$d_6$ and deuterated phosphate buffer (9:1, *v*/*v*) at pH 6.8 with $H_2O_2$ (100 mM) at 25 °C (PBCA concentration = 13 mg/mL). QM was characterized as hydroxybenzyl alcohol, as QM could easily react with nucleophilic $H_2O$ to generate hydroxybenzyl alcohol.[39] As shown in Figure 1B, the proton resonance signals at 2.81−2.87 ppm (*a*) changed to 2.99−3.08 ppm in the presence of $H_2O_2$. The proton resonance signals at 7.75−7.78 ppm (*b*) and 7.37−7.40 ppm (*c*) gradually diminished from 0 to 96 h, while two new peaks at 7.08−7.11 ppm (*c*′) and 6.68−6.71 ppm (*b*′) appeared as well as the shift of the benzylic proton at the para position from phenylboronic acid (*d*) at $\delta$ 5.8 ppm to (*d*′) at $\delta$ 5.65 ppm. The changes of chemical shifts for protons *b* and *c* should be attributed to the structural change of PBCA upon $H_2O_2$ oxidation. In addition, the proton resonance signals at 4.89 ppm (*e*) gradually diminished, and new peaks at 4.75 ppm (*f*′) and 10.37 ppm (*g*′) appeared, demonstrating the generation of CA in the acidic condition. We further tested the CA release from the TSEOP using dialysis method. As shown in Figure 1C, the release rate of CA was faster at pH 6.8 compared to that at pH 7.4, which was attributed to accelerated hydrolysis of acetal bond at acidic condition. The presence of $H_2O_2$ facilitates the detachment of boric acid group and subsequent intramolecular rearrangement,[40] which will produce QM and accelerate the hydrolysis of acetal and CA release. There was about 70% of total amount CA released from TSEOP in 96 h at pH 6.8 with 100 $\mu$M $H_2O_2$, and nearly 100% of CA released in 96 h at pH 6.8 with 10 mM $H_2O_2$. Since tumor cells and tumor extracellular matrix generally have much higher $H_2O_2$ concentration than normal cells and tumor tissues,[34,41,42] TSEOP may have preferential activity to tumor cells than to normal cells. The changes in nanostructure after the generation of CA and QM were confirmed by TEM, and the self-assembled TSEOP nanomicelles presented spherical morphologies after incubated in pH 6.8 PB with 100 mM for 0 h. However, the morphologies of nanomicelles changed into


https://dx.doi.org/10.1021/acs.nanolett.9b05265
Nano Lett. XXXX, XXX, XXX−XXX

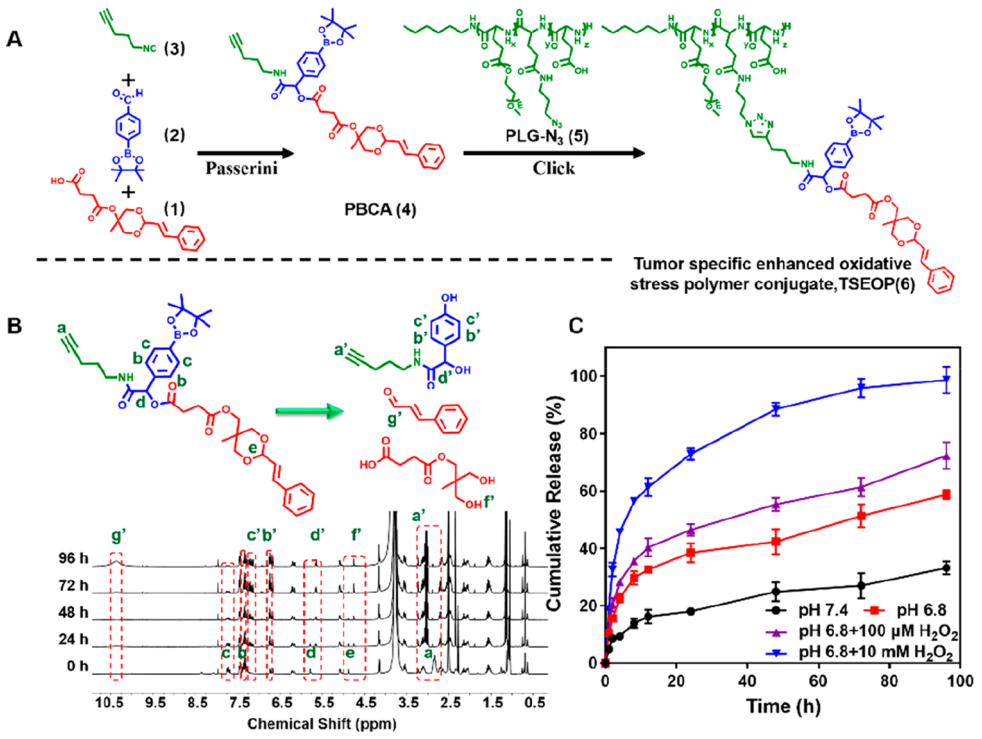


**Figure 1.** Synthesis route of TSEOP and stimuli responsive release of CA and QM. (A) Synthesis route of TSEOP. (B) $^1$H NMR test for $H_2O_2$-responsive disassociation of PBCA, with the formation of 4-hydroxybenzyl alcohol from released QM as well as the release of CA after incubation in a mixture of DMSO-$d_6$/deuterated PB (9/1, *v*/*v*, 13 mg/mL, pH = 6.8) with $H_2O_2$ (100 mM) at 25 °C. (C) *In vitro* CA release profiles of TSEOP in PBS containing 0.2% (*w*/*v*) Tween 80 at various conditions: pH 7.4, pH 6.8, pH 6.8 with 100 $\mu$M $H_2O_2$ and pH 6.8 with 10 mM $H_2O_2$, mean ± S.D., $n$ = 3.

irregular and vague shapes as the incubation time extended to 24 h (Figure S9C).

CA is a commercial food additive approved by the Food and Drug Administration (FDA) and has been reported to induce generation of ROS mainly in the mitochondria by depleting intracellular thiols.[43,44] We first evaluated the endocytosis of TSEOP by flow cytometry with Cy5 labeled TSEOP (Cy5-TSEOP). As shown in Figure S10, TSEOP could be effectively endocytosed by CT26 cells, and more TSEOP was endocytosed as time extended. The effect of TSEOP on intracellular ROS and GSH levels was further evaluated in CT26 cells. To evaluate the cooperative effect of the released QM and CA in the TSEOP, P-CA (PLG-*g*-mPEG directly conjugated with acetal modified CA, Figure S11) and P-PBA (PLG-*g*-mPEG directly conjugated with 4-(hydroxymethyl) phenylboronic acid, Figure S12) were prepared as control polymers. Intracellular ROS level was measured using dichlorofluorescein-diacetate (DCFH-DA) as a fluorescent probe. As shown in Figure 2A and B, TSEOP treatment could significantly increase the intracellular ROS level, as much stronger intracellular green fluorescence was observed compared to free CA or P-CA. The superior ROS induction property of TSEOP was largely attributed to synergistic effect of ROS generation induced by CA and GSH depletion induced by QM. Tumor cells will produce GSH to balance intracellular redox equilibrium.[45] The influence of TSEOP on intracellular GSH level was also evaluated. A much lower intracellular GSH level was detected after the treatment of TSEOP compared to that of free CA and P-CA (Figure 2C). The GSH depletion effect was mainly attributed to the PBA group in the TSEOP, as free PBA and P-PBA could decrease the intracellular GSH levels (Figure 2D). The above results indicated that TSEOP can significantly increase the cellular oxidative stress by cooperative generation of ROS and depletion of GSH.

As elevated cellular ROS and oxidative stress would induce cell apoptosis, we investigated the cytotoxicity of TSEOP against both tumor cells and normal cells.[46] As shown in Figure S13A, TSEOP resulted in higher percentage of cell apoptosis in CT26 cells compared with free CA and P-CA. At 24 h, the IC50 values of TSEOP to CT26 cells and 4T1 cells were 31.53 and 27.87 $\mu$g/mL, respectively, while the IC50 values of free CA and P-CA were both over 100 $\mu$g/mL (Figures 2E and S13B). It should be noted that the toxicity of TSEOP to normal cells (3T3 fibroblasts) at the same condition is much lower, and there is no significant difference among TSEOP with CA and P-CA (Figure 2F). There might be two reasons for the toxicity difference between tumor cells and normal cells: (1) the pH and $H_2O_2$ sensitive design in TSEOP make the release of CA and QM in normal cells slower than that in tumor cells;[47,48] (2) normal cells are generally not as sensitive to oxidative stress as tumor cells.[37,49]

To test the potential of TSEOP in inducing ICD, CRT expose, HMGB1, and ATP release, the three key markers for ICD, were tested in CT26 cells. As shown in Figure 2G and H, HMGB1 and ATP release was much elevated after TSEOP treatment. In addition, much increased CRT positive CT26 population was observed after treatment with TSEOP for 4 h, while free CA or P-CA did not show such effect at the same CA concentration (Figure 2I). As HMGB1 serves as a Toll-like receptor 4 agonist, we further tested the bone marrow-derived dendritic cells (BMDCs) activation with the culture medium of CT26 cells after various treatments. The CD80 expression was much elevated on DCs treated with the culture medium of tumor cells treated with TSEOP, suggesting effective activation


https://dx.doi.org/10.1021/acs.nanolett.9b05265
Nano Lett. XXXX, XXX, XXX−XXX

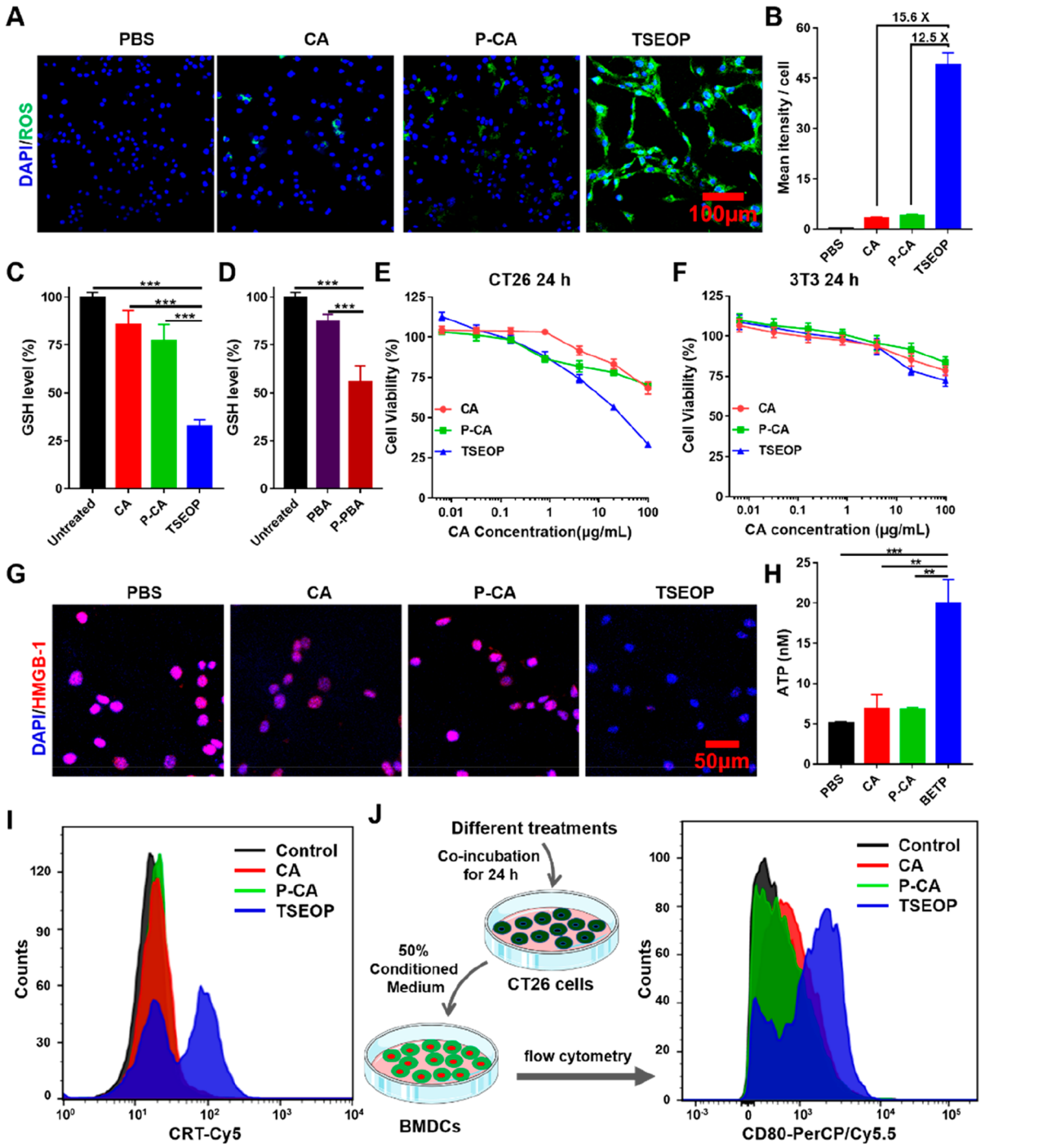


**Figure 2.** TSEOP induced oxidative stress and ICD of tumor cells *in vitro*. (A) Confocal laser scanning microscope (CLSM) images of CT26 cells treated with PBS, CA, P-CA, TSEOP at a CA concentration of 50 $\mu$M for 24 h. ROS levels were determined using the fluorescent probe DCFH-DA (green, DCFH; blue, DAPI). (B) Relative quantification of intracellular ROS generation, $n = 3$. (C) GSH level of untreated CT26 cells and the cells treated with free CA, P-CA or TSEOP at a CA concentration of 50 $\mu$M for 24 h, $n = 3$. (D) GSH level of untreated CT26 cells and the cells treated with free PBA or P-PBA at a PBA concentration of 50 $\mu$M for 24 h, $n = 3$. (E) *In vitro* cytotoxicities of CA, P-CA, and TSEOP to CT26 cells at different CA concentrations after incubation for 24 h, $n = 5$. (F) *In vitro* cytotoxicities of CA, P-CA, and TSEOP to NIH-3T3 cells at different CA concentrations after incubation for 24 h, $n = 5$. (G) CLSM examination HMGB1 release of CT26 cells after incubation with free CA, P-CA, and TSEOP at CA concentration of 30 $\mu$g/mL for 24 h. (H) ATP release of CT26 cells after incubation with free CA, P-CA, and TSEOP at CA concentration of 30 $\mu$g/mL for 24 h, $n = 3$. (I) Flow cytometric examination of CRT positive ratio of CT26 cells after incubation with free CA, P-CA, and TSEOP at CA concentration of 100 $\mu$g/mL for 4 h. (J) Schematic illustration of *in vitro* DCs activation experiment and the flow cytometry results, $n = 3$. The data are expressed as mean ± SD, ** $p < 0.01$, ***$p < 0.001$.

of DCs (Figure 2J). The above results confirmed that TSEOP treatment could effectively induce ICD and stimulate antigen presenting cells activation.

Inspired by *in vitro* results, we further evaluated the *in vivo* performance of TSEOP. First, the pharmacokinetics of TSEOP was evaluated in SD rats using Cy5-TSEOP. As shown in


https://dx.doi.org/10.1021/acs.nanolett.9b05265
Nano Lett. XXXX, XXX, XXX−XXX

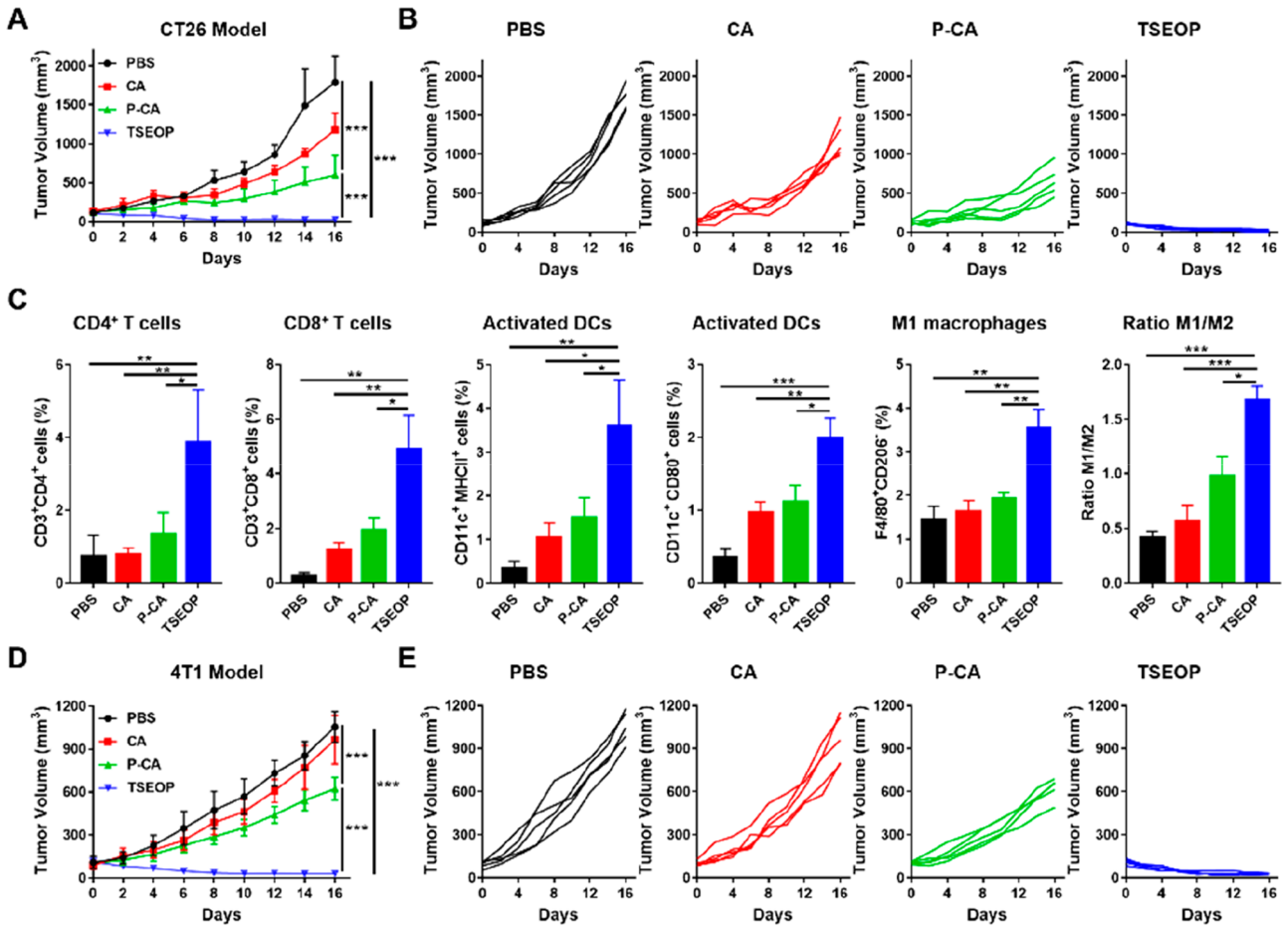


**Figure 3.** *In vivo* antitumor effects in CT26 and 4T1 tumor models. (A) Tumor volumes of CT26 tumors after various treatments; $n = 5$. (B) Individual CT26 tumor growth curves after receiving various treatments. (C) Flow cytometry results of CT26 tumors after receiving various treatments; $n = 3$. (D) Tumor volumes of 4T1 tumors after various treatments; $n = 5$. (E) Individual 4T1 tumor growth curves after receiving various treatments. Results are presented as means ± SD; $* p < 0.05$, $** p < 0.01$, $***p < 0.001$.

Figure S14, TSEOP has relatively long circulation in blood, and the biological half-life ($t_{1/2}$) of TSEOP is estimated as 12.01 ± 1.27 h, with the $AUC_{0-t}$ of 7905.26 ± 1018.16 μg/mL h in 24 h. Biodistribution study showed that liver and tumor were the major accumulation organs for TSEOP at 24 h post injection in CT26 tumor model (Figure S15).

The *in vivo* antitumor performance of TSEOP was first evaluated in the CT26 model. Once the tumor volumes reached about 100 $mm^3$, mice received the treatment of PBS, free CA, P-CA, or TSEOP at a dosage of 10 mg/kg on CA basis on day 0, 3, 6, and 9. As shown in Figure 3A and B, TSEOP effectively inhibited tumor growth and almost completely eradicated the tumor by the end of the observation, while free CA and P-CA only resulted in 32.1% and 61.6% tumor suppression rate (TSR%). In addition, a much wider apoptosis region was observed in the TdT-mediated dUTP nick-end labeling (TUNEL) assay (Figure S16) and HE staining in TSEOP treated group (Figure S17). We further evaluated the tumor immune microenvironment changes after various treatments with flow cytometry (Figures 3C and S18). After TSEOP treatment, more $CD4^+$ T cells (3.9% of total cells) and $CD8^+$ T cells (4.9% of total cells) were detected inside the tumor. More activated DCs (characterized by $MHCII^+$ and $CD80^+$ populations among the $CD11c^+$ populations) was also observed, suggesting effective immune activation by the TSEOP treatment. In addition, the TAMs composition inside the tumor was also changed: the ratio of M1 over M2 macrophages was increased in the TSEOP treatment group. To prove that the antitumor effect and the immune response induced by TSEOP could be extended to other types of cancer, we evaluated the therapeutic effect of TSEOP on 4T1 triple negative breast cancer. Similar to the treatment in CT26 model, we gave the 4T1 tumor bearing mice with PBS, free CA, P-CA, or TSEOP at a 3 day intervals for a total of four times treatments. As shown in Figure 3D and E, the 4T1 tumor was also completely eradicated on day 16. Similarly, TSEOP treatment greatly changed the immune microenvironment, with much increased $CD3^+CD8^+$ T cells, $CD3^+CD4^+$T cells, activated DCs, and increased M1/M2 ratios (Figures S19 and S20).

The outstanding tumor inhibition effect of TSEOP could be atributed to two major reasons: (1) TSEOP induced cooperative strong oxidative stress leads to large population of apoptosis of tumor cells; (2) TSEOP induced ICD leads to much increased T cell infiltration inside the tumor and strong antitumor immunity. To prove whether TSEOP could elicit a tumor-specific antitumor immunity *in vivo*, we conducted a vaccination and rechallenge experiment in CT26 model. BALB/c mice were first immunized twice with PBS, fresh CT26 cells, or CT26 cells pretreated with TSEOP (TSEOP-CT26 cells) on day −7 and day −1, and then $1 \times 10^6$ CT26 cells were challenged on the other flank of each mouse on day


https://dx.doi.org/10.1021/acs.nanolett.9b05265
Nano Lett. XXXX, XXX, XXX−XXX

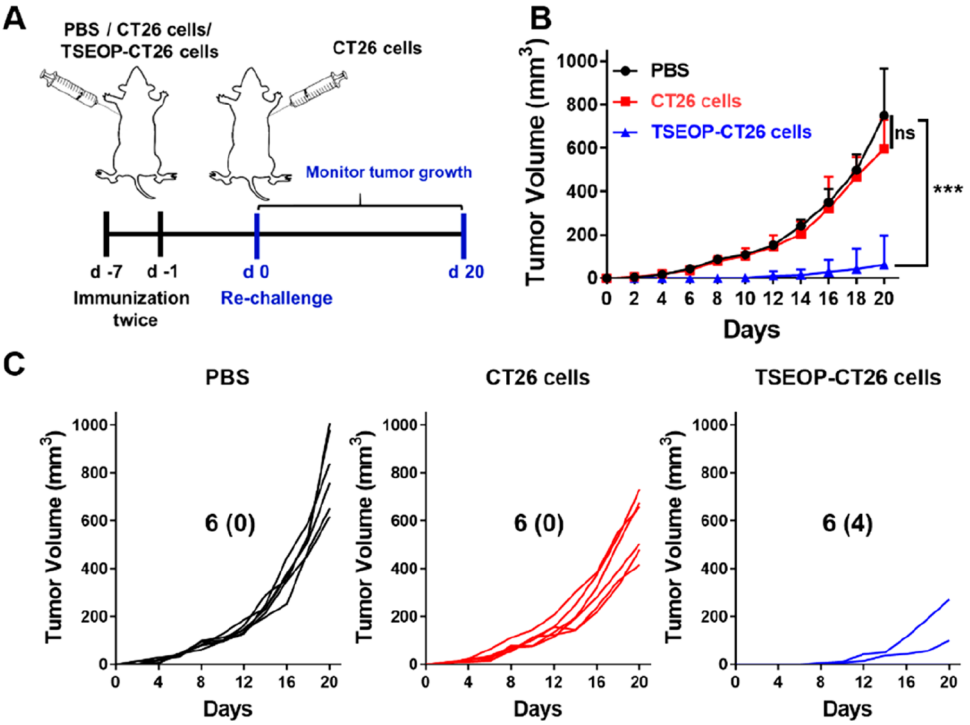


**Figure 4.** Vaccination and rechallenge experiments to evaluate the *in vivo* tumor-specific immunity induced TSEOP. (A) Schematic of vaccination and rechallenge experiment design. (B) Tumor volume curves of rechallenged tumors after mice receiving various vaccination: PBS, CT26 cells, TSEOP-CT26 cells. (C) Individual rechallenged tumor growth curves after receiving various immunization. Results are presented as means ± SD; ***$p < 0.001$, ns, no significance.

0 (Figure 4A). As shown in Figure 4B and C, the newly incubated CT26 tumor cells grow fast in mice immunized with PBS and CT26 cells, while much slower in the mice immunized with TSEOP-CT26 cells, and 4 out of 6 mice were still tumor free on day 20. All these results confirmed that TSEOP therapy could effectively activate tumor-specific antitumor immunity and effectively inhibit tumor growth *in vivo*.

The safety profiles of the TSEOP treatment were also evaluated. No obvious body weight loss was observed after various treatments (Figure S21). In addition, no obvious damage was observed in HE analysis of the major organs of the mice (Figure S22), and blood chemistry analysis showed no obvious changes in ALT/AST/UA/CREA, indicating that the treatment of TSEOP did not cause any significant liver or kidney function changes (Figure S23). All these results demonstrated that the treatment of TSEOP was safe and effective and showed great potential for the clinical translation.

**Conclusions.** In summary, we present a safe and effective approach to utilize polymer based therapeutics to inhibit tumor growth and enhance cancer immunotherapy. With well-tailored structure, the rationally designed TSEOP could specifically and cooperatively increase oxidative stress in tumor cells and subsequently lead to effective ICD to the tumor cells without killing the normal cells. The *in vivo* results demonstrated that single TSEOP treatment could eradicate both CT26 colon tumor and 4T1 tripal negative breast tumors. Detailed investigation showed that TSEOP effectively activated immune systems *in vivo* with more $CD3^+CD8^+$ T cells and activated DCs and M1 macrophages infiltration. Vaccination and rechallenge experiment confirmed the TSEOP could induce tumor-specific antitumor immunity *in vivo*. With excellent tumor selectivity and superior antitumor efficacy, the TSEOP renders a new approach for designing polymer based cancer immunotherapeutics and may also serve as a safe and cost-effective modality for cancer immunotherapy.

## ■ ASSOCIATED CONTENT

### Supporting Information

The Supporting Information is available free of charge at https://pubs.acs.org/doi/10.1021/acs.nanolett.9b05265.

Detailed synthesis procedures, NMR spectra, GPC spectrum, TUNEL and HE staining, other supplementary data (PDF)

## ■ AUTHOR INFORMATION


### Corresponding Authors

**Wantong Song** − *Key Laboratory of Polymer Ecomaterials, Changchun Institute of Applied Chemistry, Chinese Academy of Sciences, Changchun 130022, China; Jilin Biomedical Polymers Engineering Laboratory, Changchun 130022, China; State Key Laboratory of Molecular Engineering of Polymers (Fudan University), Shanghai 200433, China;* orcid.org/0000-0002-4564-9917; Email: wtsong@ciac.ac.cn

**Xuesi Chen** − *Key Laboratory of Polymer Ecomaterials, Changchun Institute of Applied Chemistry, Chinese Academy of Sciences, Changchun 130022, China; University of Science and Technology of China, Hefei 230026, China; Jilin Biomedical Polymers Engineering Laboratory, Changchun 130022, China;* orcid.org/0000-0003-3542-9256; Email: xschen@ciac.ac.cn

### Authors

**Sheng Ma** − *Key Laboratory of Polymer Ecomaterials, Changchun Institute of Applied Chemistry, Chinese Academy of Sciences, Changchun 130022, China; University of Science and*




https://dx.doi.org/10.1021/acs.nanolett.9b05265
Nano Lett. XXXX, XXX, XXX−XXX

*Technology of China, Hefei 230026, China; Jilin Biomedical Polymers Engineering Laboratory, Changchun 130022, China*

**Yudi Xu** − *Key Laboratory of Polymer Ecomaterials, Changchun Institute of Applied Chemistry, Chinese Academy of Sciences, Changchun 130022, China; Jilin Biomedical Polymers Engineering Laboratory, Changchun 130022, China; University of Chinese Academy of Sciences, Beijing 100039, China*

**Xinghui Si** − *Key Laboratory of Polymer Ecomaterials, Changchun Institute of Applied Chemistry, Chinese Academy of Sciences, Changchun 130022, China; University of Science and Technology of China, Hefei 230026, China; Jilin Biomedical Polymers Engineering Laboratory, Changchun 130022, China*

**Shixian Lv** − *Department of Bioengineering, Molecular Engineering and Sciences Institute, University of Washington, Seattle, Washington 98195, United States*

**Yu Zhang** − *Key Laboratory of Polymer Ecomaterials, Changchun Institute of Applied Chemistry, Chinese Academy of Sciences, Changchun 130022, China; Jilin Biomedical Polymers Engineering Laboratory, Changchun 130022, China*

**Zhaohui Tang** − *Key Laboratory of Polymer Ecomaterials, Changchun Institute of Applied Chemistry, Chinese Academy of Sciences, Changchun 130022, China; University of Science and Technology of China, Hefei 230026, China; Jilin Biomedical Polymers Engineering Laboratory, Changchun 130022, China*

Complete contact information is available at: https://pubs.acs.org/10.1021/acs.nanolett.9b05265

### Notes

The authors declare no competing financial interest.

## ■ ACKNOWLEDGMENTS

This work is supported by the National Natural Science Foundation of China (51673185, 51973215, 51673189, 51833010, 51520105004, 51829302), the Jilin Province Science and Technology Development Plan (20190103112JH), and Ministry of Science and Technology of China (2016YFC1100701). We acknowledge Prof. Zhenxin Wang and his group member Hongda Chen from Chang Chun Institute of Applied Chemistry for the assistance in the use of Davinch Invivo HR imaging system.

## ■ REFERENCES

(1) Yu, H.; Kortylewski, M.; Pardoll, D. Crosstalk between cancer and immune cells: role of STAT3 in the tumour microenvironment. *Nat. Rev. Immunol.* **2007**, *7* (1), 41−51.

(2) Elinav, E.; Nowarski, R.; Thaiss, C. A.; Hu, B.; Jin, C. C.; Flavell, R. A. Inflammation-induced cancer: crosstalk between tumours, immune cells and microorganisms. *Nat. Rev. Cancer* **2013**, *13* (11), 759−771.

(3) Mantovani, A.; Allavena, P.; Sica, A.; Balkwill, F. Cancer-related inflammation. *Nature* **2008**, *454* (7203), 436−444.

(4) Joyce, J. A.; Pollard, J. W. Microenvironmental regulation of metastasis. *Nat. Rev. Cancer* **2009**, *9* (4), 239−252.

(5) Noy, R.; Pollard, J. W. Tumor-Associated Macrophages: From Mechanisms to Therapy. *Immunity* **2014**, *41* (1), 49−61.

(6) Fridlender, Z. G.; Sun, J.; Kim, S.; Kapoor, V.; Cheng, G. J.; Ling, L. N.; Worthen, G. S.; Albelda, S. M. Polarization of Tumor-Associated Neutrophil Phenotype by TGF-beta: "N1" versus "N2" TAN. *Cancer Cell* **2009**, *16* (3), 183−194.

(7) Song, W.; Tiruthani, K.; Wang, Y.; Shen, L.; Hu, M.; Dorosheva, O.; Qiu, K.; Kinghorn, K. A.; Liu, R.; Huang, L. Trapping of Lipopolysaccharide to Promote Immunotherapy against Colorectal Cancer and Attenuate Liver Metastasis. *Adv. Mater.* **2018**, *30* (52), 1805007.

(8) Sharma, A.; Lee, M.-G.; Won, M.; Koo, S.; Arambula, J. F.; Sessler, J. L.; Chi, S.-G.; Kim, J. S. Targeting Heterogeneous Tumors Using a Multifunctional Molecular Prodrug. *J. Am. Chem. Soc.* **2019**, *39*, 15611−15618.

(9) Chen, Y.; Song, W.; Shen, L.; Qiu, N.; Hu, M.; Liu, Y.; Liu, Q.; Huang, L. Vasodilator Hydralazine Promotes Nanoparticle Penetration in Advanced Desmoplastic Tumors. *ACS Nano* **2019**, *13* (2), 1751−1763.

(10) Song, W.; Shen, L.; Wang, Y.; Liu, Q.; Goodwin, T. J.; Li, J.; Dorosheva, O.; Liu, T.; Liu, R.; Huang, L. Synergistic and low adverse effect cancer immunotherapy by immunogenic chemotherapy and locally expressed PD-L1 trap. *Nat. Commun.* **2018**, *9*, 2237−2247.

(11) Feng, B.; Zhou, F.; Hou, B.; Wang, D.; Wang, T.; Fu, Y.; Ma, Y.; Yu, H.; Li, Y. Binary Cooperative Prodrug Nanoparticles Improve Immunotherapy by Synergistically Modulating Immune Tumor Microenvironment. *Adv. Mater.* **2018**, *30* (38), 1803001.

(12) Song, W.; Das, M.; Xu, Y.; Si, X.; Zhang, Y.; Tang, Z.; Chen, X. Leveraging biomaterials for cancer immunotherapy: targeting pattern recognition receptors. *Materials Today Nano* **2019**, *5*, 100029.

(13) Casares, N.; Pequignot, M. O.; Tesniere, A.; Ghiringhelli, F.; Roux, S.; Chaput, N.; Schmitt, E.; Hamai, A.; Hervas-Stubbs, S.; Obeid, M.; Coutant, F.; Metivier, D.; Pichard, E.; Aucouturier, P.; Pierron, G.; Garrido, C.; Zitvogel, L.; Kroemer, G. Caspase-dependent immunogenicity of doxorubicin-induced tumor cell death. *J. Exp. Med.* **2005**, *202* (12), 1691−1701.

(14) Hanayama, R.; Tanaka, M.; Miwa, K.; Shinohara, A.; Iwamatsu, A.; Nagata, S. Identification of a factor that links apoptotic cells to phagocytes. *Nature* **2002**, *417* (6885), 182−187.

(15) Taha, M. S.; Cresswell, G. M.; Park, J.; Lee, W.; Ratliff, T. L.; Yeo, Y. Sustained Delivery of Carfilzomib by Tannic Acid-Based Nanocapsules Helps Develop Antitumor Immunity. *Nano Lett.* **2019**, *19* (11), 8333−8341.

(16) Qi, J.; Li, W.; Lu, K.; Jin, F.; Liu, D.; Xu, X.; Wang, X.; Kang, X.; Wang, W.; Shu, G.; Han, F.; Ying, X.; You, J.; Ji, J.; Du, Y. pH and Thermal Dual-Sensitive Nanoparticle-Mediated Synergistic Antitumor Effect of Immunotherapy and Microwave Thermotherapy. *Nano Lett.* **2019**, *19* (8), 4949−4959.

(17) Huang, H.; Jiang, C. T.; Shen, S.; Liu, A.; Gang, Y. J.; Tong, Q. S.; Chen, S. B.; Gao, Z. X.; Du, J. Z.; Cao, J.; Wang, J. Nanoenabled Reversal of IDO1-Mediated Immunosuppression Synergizes with Immunogenic Chemotherapy for Improved Cancer Therapy. *Nano Lett.* **2019**, *19* (8), 5356−5365.

(18) Liu, P.; Zhao, L. W.; Pol, J.; Levesque, S.; Petrazzuolo, A.; Pfirschke, C.; Engblom, C.; Rickelt, S.; Yamazaki, T.; Iribarren, K.; Senovilla, L.; Bezu, L.; Vacchelli, E.; Sica, V.; Melis, A.; Martin, T.; Lin, X.; Yang, H.; Li, Q. Q.; Chen, J. F.; Durand, S.; Aprahamian, F.; Lefevre, D.; Broutin, S.; Paci, A.; Bongers, A.; Minard-Colin, V.; Tartour, E.; Zitvogel, L.; Apetoh, L.; Ma, Y. T.; Pittet, M. J.; Kepp, O.; Kroemer, G. Crizotinib-induced immunogenic cell death in non-small cell lung cancer. *Nat. Commun.* **2019**, *10*, 1486−1502.

(19) Basu, S.; Srivastava, P. K. Calreticulin, a peptide-binding chaperone of the endoplasmic reticulum, elicits tumor- and peptide-specific immunity. *J. Exp. Med.* **1999**, *189* (5), 797−802.

(20) Zitvogel, L.; Kepp, O.; Senovilla, L.; Menger, L.; Chaput, N.; Kroemer, G. Immunogenic Tumor Cell Death for Optimal Anticancer Therapy: The Calreticulin Exposure Pathway. *Clin. Cancer Res.* **2010**, *16* (12), 3100−3104.

(21) Zhang, K.; Kaufman, R. J. From endoplasmic-reticulum stress to the inflammatory response. *Nature* **2008**, *454* (7203), 455−462.

(22) Srinivas, U. S.; Tan, B. W. Q.; Vellayappan, B. A.; Jeyasekharan, A. D. ROS and the DNA damage response in cancer. *Redox Biol.* **2019**, *25*, 101084.

(23) Krysko, D. V.; Garg, A. D.; Kaczmarek, A.; Krysko, O.; Agostinis, P.; Vandenabeele, P. Immunogenic cell death and DAMPs in cancer therapy. *Nat. Rev. Cancer* **2012**, *12* (12), 860−875.

(24) Wang, G.; Zhang, D.; Yang, S.; Wang, Y.; Tang, Z.; Fu, X. Co-administration of genistein with doxorubicin-loaded polypeptide nanoparticles weakens the metastasis of malignant prostate cancer by amplifying oxidative damage. *Biomater. Sci.* **2018**, *6* (4), 827−835.



https://dx.doi.org/10.1021/acs.nanolett.9b05265
*Nano Lett.* XXXX, XXX, XXX−XXX

(25) Kim, S. J.; Kim, M. S.; Lee, J. W.; Lee, C. H.; Yoo, H.; Shin, S. H.; Park, M. J.; Lee, S. H. Dihydroartemisinin enhances radiosensitivity of human glioma cells in vitro. *J. Cancer Res. Clin. Oncol.* **2006**, *132* (2), 129−135.
(26) Wang, N. N.; Zhao, Z. L.; Lv, Y. F.; Fan, H. H.; Bai, H. R.; Meng, H. M.; Long, Y. Q.; Fu, T.; Zhang, X. B.; Tan, W. H. Gold nanorod-photosensitizer conjugate with extracellular pH-driven tumor targeting ability for photothermal/photodynamic therapy. *Nano Res.* **2014**, *7* (9), 1291−1301.
(27) Azzam, E. I.; Jay-Gerin, J.-P.; Pain, D. Ionizing radiation-induced metabolic oxidative stress and prolonged cell injury. *Cancer Lett.* **2012**, *327* (1−2), 48−60.
(28) Wang, K.; Zhang, Z.; Lin, L.; Chen, J.; Hao, K.; Tian, H.; Chen, X. Covalent Organic Nanosheets Integrated Heterojunction with Two Strategies To Overcome Hypoxic-Tumor Photodynamic Therapy. *Chem. Mater.* **2019**, *31* (9), 3313−3323.
(29) Lu, K.; He, C.; Guo, N.; Chan, C.; Ni, K.; Weichselbaum, R. R.; Lin, W. Chlorin-Based Nanoscale Metal-Organic Framework Systemically Rejects Colorectal Cancers via Synergistic Photodynamic Therapy and Checkpoint Blockade Immunotherapy. *J. Am. Chem. Soc.* **2016**, *138* (38), 12502−12510.
(30) Lan, G.; Ni, K.; Xu, Z.; Veroneau, S. S.; Song, Y.; Lin, W. Nanoscale Metal-Organic Framework Overcomes Hypoxia for Photodynamic Therapy Primed Cancer Immunotherapy. *J. Am. Chem. Soc.* **2018**, *140* (17), 5670−5673.
(31) Feng, B.; Hou, B.; Xu, Z.; Saeed, M.; Yu, H.; Li, Y. Self-Amplified Drug Delivery with Light-Inducible Nanocargoes to Enhance Cancer Immunotherapy. *Adv. Mater.* **2019**, *31*, 1902960.
(32) Robertson, C. A.; Evans, D. H.; Abraharnse, H. Photodynamic therapy (PDT): A short review on cellular mechanisms and cancer research applications for PDT. *J. Photochem. Photobiol., B* **2009**, *96* (1), 1−8.
(33) Li, J.; Dirisala, A.; Ge, Z.; Wang, Y.; Yin, W.; Ke, W.; Toh, K.; Xie, J.; Matsumoto, Y.; Anraku, Y.; Osada, K.; Kataoka, K. Therapeutic Vesicular Nanoreactors with Tumor-Specific Activation and Self-Destruction for Synergistic Tumor Ablation. *Angew. Chem., Int. Ed.* **2017**, *56* (45), 14025−14030.
(34) Li, J.; Li, Y.; Wang, Y.; Ke, W.; Chen, W.; Wang, W.; Ge, Z. Polymer Prodrug-Based Nanoreactors Activated by Tumor Acidity for Orchestrated Oxidation/Chemotherapy. *Nano Lett.* **2017**, *17* (11), 6983−6990.
(35) Yin, W.; Ke, W.; Chen, W.; Xi, L.; Zhou, Q.; Mukerabigwi, J. F.; Ge, Z. Integrated block copolymer prodrug nanoparticles for combination of tumor oxidative stress amplification and ROS-responsive drug release. *Biomaterials* **2019**, *195*, 63−74.
(36) Yin, W.; Li, J.; Ke, W.; Zha, Z.; Ge, Z. Integrated Nanoparticles To Synergistically Elevate Tumor Oxidative Stress and Suppress Antioxidative Capability for Amplified Oxidation Therapy. *ACS Appl. Mater. Interfaces* **2017**, *9* (35), 29538−29546.
(37) Gong, N.; Ma, X.; Ye, X.; Zhou, Q.; Chen, X.; Tan, X.; Yao, S.; Huo, S.; Zhang, T.; Chen, S.; Teng, X.; Hu, X.; Yu, J.; Gan, Y.; Jiang, H.; Li, J.; Liang, X.-J. Carbon-dot-supported atomically dispersed gold as a mitochondrial oxidative stress amplifier for cancer treatment. *Nat. Nanotechnol.* **2019**, *14* (4), 379−389.
(38) Yu, H. Y.; Tang, Z. H.; Li, M. Q.; Song, W. T.; Zhang, D. W.; Zhang, Y.; Yang, Y.; Sun, H.; Deng, M. X.; Chen, X. S. Cisplatin Loaded Poly(L-glutamic acid)-g-Methoxy Poly(ethylene glycol) Complex Nanoparticles for Potential Cancer Therapy: Preparation, In Vitro and In Vivo Evaluation. *J. Biomed. Nanotechnol.* **2016**, *12* (1), 69−78.
(39) Hagen, H.; Marzenell, P.; Jentzsch, E.; Wenz, F.; Veldwijk, M. R.; Mokhir, A. Aminoferrocene-Based Prodrugs Activated by Reactive Oxygen Species. *J. Med. Chem.* **2012**, *55* (2), 924−934.
(40) Lv, S.; Wu, Y.; Cai, K.; He, H.; Li, Y.; Lan, M.; Chen, X.; Cheng, J.; Yin, L. High Drug Loading and Sub-Quantitative Loading Efficiency of Polymeric Micelles Driven by Donor-Receptor Coordination Interactions. *J. Am. Chem. Soc.* **2018**, *140* (4), 1235−1238.
(41) Chen, Q.; Liang, C.; Sun, X.; Chen, J.; Yang, Z.; Zhao, H.; Feng, L.; Liu, Z. H2O2-responsive liposomal nanoprobe for photoacoustic inflammation imaging and tumor theranostics via in vivo chromogenic assay. *Proc. Natl. Acad. Sci. U. S. A.* **2017**, *114* (21), 5343−5348.
(42) Szatrowski, T. P.; Nathan, C. F. PRODUCTION OF LARGE AMOUNTS OF HYDROGEN-PEROXIDE BY HUMAN TUMOR-CELLS. *Cancer Res.* **1991**, *51* (3), 794−798.
(43) Ka, H.; Park, H. J.; Jung, H. J.; Choi, J. W.; Cho, K. S.; Ha, J.; Lee, K. T. Cinnamaldehyde induces apoptosis by ROS-mediated mitochondrial permeability transition in human promyelocytic leukemia HL-60 cells. *Cancer Lett.* **2003**, *196* (2), 143−152.
(44) Hong, S. H.; Kim, J.; Kim, J.-M.; Lee, S.-Y.; Shin, D.-S.; Son, K.-H.; Han, D. C.; Sung, Y. K.; Kwon, B.-M. Apoptosis induction of 2′-hydroxycinnamaldehyde as a proteasorne inhibitor is associated with ER stress and mitochondrial perturbation in cancer cells. *Biochem. Pharmacol.* **2007**, *74* (4), 557−565.
(45) Diehn, M.; Cho, R. W.; Lobo, N. A.; Kalisky, T.; Dorie, M. J.; Kulp, A. N.; Qian, D.; Lam, J. S.; Ailles, L. E.; Wong, M.; Joshua, B.; Kaplan, M. J.; Wapnir, I.; Dirbas, F. M.; Somlo, G.; Garberoglio, C.; Paz, B.; Shen, J.; Lau, S. K.; Quake, S. R.; Brown, J. M.; Weissman, I. L.; Clarke, M. F. Association of reactive oxygen species levels and radioresistance in cancer stem cells. *Nature* **2009**, *458* (7239), 780−785.
(46) Song, J.; Lin, L.; Yang, Z.; Zhu, R.; Zhou, Z.; Li, Z.-W.; Wang, F.; Chen, J.; Yang, H.; Chen, X. Self-Assembled Responsive Bilayered Vesicles with Adjustable Oxidative Stress for Enhanced Cancer Imaging and Therapy. *J. Am. Chem. Soc.* **2019**, *141* (20), 8158−8170.
(47) Sun, R.; Qiu, N. S.; Shen, Y. Q. Polymeric Cancer Nanomedicines: Challenge and Development. *Acta Polym. Sin.* **2019**, *50* (6), 588−601.
(48) Li, H.-J.; Liu, J.; Luo, Y.-L.; Chen, S.-B.; Liu, R.; Du, J.-Z.; Wang, J. Intratumor Performance and Therapeutic Efficacy of PAMAM Dendrimers Carried by Clustered Nanoparticles. *Nano Lett.* **2019**, *19* (12), 8947−8955.
(49) Trachootham, D.; Alexandre, J.; Huang, P. Targeting cancer cells by ROS-mediated mechanisms: a radical therapeutic approach? *Nat. Rev. Drug Discovery* **2009**, *8* (7), 579−591.


https://dx.doi.org/10.1021/acs.nanolett.9b05265
*Nano Lett.* XXXX, XXX, XXX−XXX